Clays and Clay Minerals, Vol. 56, No. 3, 359–379, 2008.

EARLY CLAY DIAGENESIS IN GULF COAST SEDIMENTS: NEW INSIGHTS FROM XRD PROFILE MODELING

DOUGLAS K. MCCARTY[1,*], BORIS A. SAKHAROV[2], AND VICTOR A. DRITS[2]

[1] Chevron ETC, 3901 Briarpark, Houston, TX, 77063 USA
[2] Geological Institute of the Russian Academy of Science, Pyzevskij per. D.7, 119017 Moscow, Russia

Abstract—Samples from different depths in the Oligocene Frio formation (offshore Gulf of Mexico) were studied by X-ray diffraction (XRD), thermal analyses, and scanning electron microscopy. The experimental XRD patterns recorded from oriented and ethylene glycol (EG) solvated clay fractions of the samples were similar to those typical of random, mixed-layered illite-smectite (R0 I-S). The experimental XRD patterns recorded in air-dried (AD) and EG states were simulated using three different models. One of them corresponds to R0 I-S for which thickness and content of the interstratified layers were determined by the Środoń technique. The second model is represented by a single homogeneous I-S in which illite and smectite layers are interstratified with a tendency to segregation. The expandability of the segregated I-S model varies from 48% to 75% without any rational relationship between the smectite layer content and depth.

The third model assumes that the clay fraction is a physical mixture of smectite and an R0 I-S. In this model the I-S contains 65% illite and 35% smectite layers independent of depth, whereas the smectite content varies from 28% to 63%. This model has consistently smaller profile factors, R_p, for both EG and AD XRD scans compared with the R_p values determined for the other two models.

The mineralogical association, volcanic origin, narrow stratigraphic interval (427 m), and low maximum temperature (42ºC) of the studied Frio Formation are considered. These features are completely consistent with the two-phase model and so the segregation model must be rejected. An authigenic origin of the pure smectite and an alternative detrital or authigenic origin of the R0 I-S are discussed.

Key Words—Diagenesis, Gulf Coast, Illite-Smectite, Frio Formation, Smectite.

INTRODUCTION

The study of the smectite illitization reaction during burial diagenesis attracts special attention for several reasons. One is that this reaction is accompanied by the maturation, migration, and trapping of hydrocarbons (Burst, 1969; Hunt, 1979; Foscolos and Powell, 1979). Recently Drits *et al*. (2002a, 2002b) showed that in oil-source rocks, oil generation and transformation of smectite layers in I-S are linked in such a way that diagenesis is accompanied not by illitization but by tobelitization of the expandable layers of the former I-S, leading to the formation of illite-tobelite-smectite phases. The degree of illitization is used as a geothermometer to reconstruct the thermal history of sedimentary basins (Pollastro, 1993) and measurements of K/Ar in fundamental illite particles are effectively used for dating of clay diagenesis (Środoń, 1999a; Środoń *et al*., 2002).

The smectite illitization is a ubiquitous reaction occurring in significantly different geological environments, including sedimentary basins and active and fossil hydrothermal systems, *etc.* (Środoń, 1999b). Different authors studying smectite illitization have proposed various reaction mechanisms (Shutov *et al*., 1969; Perry and Hower, 1970; Dunoyer de Segonzac, 1970; Hower *et al*., 1976; Altaner and Ylagan, 1997; Ylagan *et al*., 2000; Środoń *et al*., 2000). Despite the numerous investigations of the smectite-to-illite transformation, many aspects of the kinetics and mechanisms of this reaction remain poorly understood (Lanson *et al.*, 2005). One of the possible reasons is related to ambiguous interpretations of experimental XRD patterns from clays containing mixtures of discrete clay minerals and mixed-layer phases. Conventionally, in most publications, interpretation of XRD patterns is confined to the analysis of the positions of basal reflections, often ignoring their intensities and profiles. This approach employs peak migration curves which represent relationships between basal-reflection positions and the proportions and mode of interstratification of the layer types (*e.g.* Środoń, 1980, 1981, 1984; Inoue *et al*., 1988; Moore and Reynolds, 1997). Because this approach is restricted to two-component systems, the model may not correspond to the actual structure (Drits, 1997, 2003). To increase the reliability of the interpretation of diffraction effects, the multispecimen XRD method was developed (Drits *et al*., 1997a, 1997b; Sakharov *et al*., 1999). This method requires that, for the same sample, XRD patterns

* E-mail address of corresponding author:
dmccarty@chevron.com
DOI: 10.1346/CCMN.2008.0560306

should be recorded after different treatments (*e.g*. Mg- and Ca-saturated specimens in AD and EG solvated states). Using computer modeling, for each such pattern an optimal agreement between the experimental and calculated intensity distributions is obtained by a trial and error procedure.

Application of the multispecimen method provides a more reliable interpretation of the experimental XRD patterns and greater accuracy in the determination of the content and actual structure of the coexisting discrete and mixed-layer phases (Lindgreen, 2000, 2002; Drits e*t al*., 2002a, 2002b; 2004; Claret *et al*., 2004; McCarty *et al*., 2004; Ferrage *et al*., 2005a, 2005b; Lanson *et al*., 2005). However, even this method does not always provide an unambiguous determination of the actual structure as several structural models may fit the experimental XRD pattern equally well (Drits, 1987; Sakharov *et al*., 1999; McCarty *et al*., 2004). In particular, Drits *et al*. (2002a, 2002b) showed that a similar agreement between the experimental and calculated XRD patterns containing 17 Å peaks (following Ca saturation and EG solvation) can be achieved using two different structural models. In one, the positions, intensities, and profiles of the basal reflections are described with a single I-S model in which smectite and illite layers are interstratified with some tendency to segregation. In the other model, the experimental XRD pattern is described successfully using a physical mixture of a pure smectite and a randomly interstratified illite-smectite (R0 I-S). In these papers it was difficult to make an unambiguous choice between these models because the quality of the agreement between the experimental and calculated patterns compared was not estimated quantitatively. The coexistence of smectite and I-S in shallow sections of different sedimentary basins is consistent with numerous TEM observations showing that this phase association is dominant in smectite-rich samples (Dong, 2005). Few published XRD studies, however, have adopted this interpretation, results presented by Claret *et al*. (2004), Lanson *et al*. (2005), McCarty (2005), and Aplin *et al*. (2006) being the exceptions.

To illustrate the potential problems in interpretation of XRD patterns containing 17 Å peaks, the present paper presents the results of a study of clay fractions of samples selected from the Upper Oligocene Frio Formation sediments which were deposited in a deep-water system. These samples were chosen because the XRD patterns of the clay fractions are similar to those typical of diagenetically transformed clays, but the clays from these sediments were not subjected to deep diagenesis and the volcanic origin of the Frio Formation is well documented (*e.g*. Lynch, 1996, 1997). These features help us to provide a reliable interpretation of the observed diffraction data, to make some conclusions concerning the origin of the clay minerals in the studied Frio Formation region, and to discuss the limitation of XRD itself in the unambiguous determination of the actual structure of smectite-rich clay minerals.

METHODS

X-ray diffraction

Quantitative X-ray phase analysis. This analysis was conducted on whole-rock samples following the procedure of Środoń *et al*. (2001), and information about the accuracy of this method may be found in Omotoso *et al*. (2006).

Clay size, oriented-aggregate sample analysis. The <2.0 μm equivalent spherical-diameter size fraction was separated from samples by standard ultrasonic disaggregation and centrifugation methods. The samples were treated to remove carbonate and Fe oxide cements with a Na-acetate buffer and Na-dithionite, respectively (Jackson, 1985). The Na^{+}-saturated clays were exchanged with Ca^{2+} and Mg^{2+} using standard methods (*e.g.* Moore and Reynolds, 1997). Oriented aggregates were made by evaporation onto glass slides to provide a sample ~4 cm long with at least 10 mg of clay per cm^2 (Moore and Reynolds, 1997). The XRD scans from these oriented preparations were compared directly with scans made from the filter-peel transfer method (Moore and Reynolds, 1997) to verify the absence of segregation of the clay phases due to differential settlement. Diffraction scans were collected with a Thermo® Xtra diffractometer equipped with a solid-state Si detector, after ethylene-glycol (EG) treatment by vapor solvation in a heated chamber (60ºC) and also in the air-dried (AD) state. Average relative humidity (RH) in the lab during the time period when the data were collected was 35% ranging from 21% to 46%. The scans were made from 2 to 52º2θ with a 0.02º2θ step increment and counting rate of 4 s per step or longer, using CuKα radiation transmitted through a 2.0 mm divergence and 4 mm scatter slit. Detector slits were 0.5 mm and 0.2 mm.

Modeling of the XRD patterns

To simulate XRD patterns from oriented clay specimens, the multispecimen method initially developed by Drits and Sakharov (1976) and later by Drits *et al*. (1997a) and Sakharov *et al*. (1999) was used. The I-S structure models include the number (not limited to 2), the nature, and the proportion of the different layer types and the statistical description of their stacking sequences. Smectite layers and interlayers containing two or one layers of EG or H_2O molecules are denoted S_1 and S_2 and correspond to 2EG and 1EG in the EG state and to 2W and 1W in the AD state, respectively. This definition allows us to account for the heterogeneous hydration or swelling behavior of expandable layers which is probably related to the amount and location of the layer charge.

Layer sequences in I-S can obey different laws which differ by the short-range order factor, R, equal to the number of the nearest preceding layers that influence the occurrence probability for a final layer of a given type. In the case of R = 0, the layer types are interstratified at random, and it is R = 1 if the occurrence of a layer of a given type depends on the nearest predecessor. To describe a layer sequence in a two-component I-S with R = 0, the relative content of each interstratified layer type, W_I and W_S should be known. In the case of R = 1, four additional junction probability parameters, P_{II}, P_{IS}, P_{SI}, and P_{SS}, are required. The value of P_{ij} defines the probability for layer type j to follow layer type i (i, j = I, S). The occurrence probability of layer pair, ij, layer triple, ijf, *etc.* are calculated by the equations $W_{ij} = W_iP_{ij}$, $W_{ijf} = W_iP_{ij}P_{jf}$ (i, j, f = I, S). The W_i and P_{ij} are interrelated and only two independent parameters are needed to describe any layer sub-sequence. In particular, when $W_I > W_S$ and R = 1 the parameters W_S and P_{SS} should be known. When $P_{SS} = 0$, layers are distributed with a maximum possible degree of order (MPDO). Such I-S is commonly referred to as R1 I-S. However, for a given W_S a set of R1 I-S varieties with some tendency to order in the layer type distribution can exist with the $W_S > P_{SS} > 0$ condition and $P_{SS} = W_S$ corresponds to I-S with R = 0. In contrast, I-S with R = 1 may exist with a variable degree of segregation of the interstratified layers that occurs when $1 > P_{SS} > W_S$. The value of $P_{SS} = 1$ corresponds to a physical mixture of illite and smectite. For a three-component model consisting, for example, of illite and two different expandable S_1 and S_2 smectite layers and $W_I > W_{S_1} > W_{S_2}$, six independent probability parameters are needed to describe layer stacking for R = 1: W_I, W_{S_1}, $P_{S_1S_1}$, $P_{S_1S_2}$, $P_{S_2S_1}$, $P_{S_2S_2}$ (see Drits and Tchoubar, 1990, for details).

Because the different treatments may change the thickness and the scattering power of expandable interlayers, but not the layer distribution within crystallites, a consistent structure model is obtained when the layer-stacking sequences are almost identical for different XRD patterns from the same sample. In addition, the relative content of the different phases determined by simulation of these patterns must be significantly similar.

Instrumental and experimental factors such as goniometer radius and the length and thickness of the oriented specimens were measured and introduced without further adjustment (Drits and Tchoubar, 1990). Sigmastar (σ^*) was set to 12º and the mass absorption coefficient (μ^*) to 45, as recommended by Moore and Reynolds (1997). For structural models of AD and EG I-S containing Mg or Ca in the interlayers, the *z* coordinates and site occupancies for 2:1 layers and interlayers of Moore and Reynolds (1997) are used. The thicknesses of the coherent scattering domains (CSDs) are lognormally distributed and the parameters of this distribution are determined using a mean thickness of CSDs and the regression given by Drits *et al*. (1997b) with mean and maximum thickness of CSDs as variable parameters.

Several structural models were tested to simulate the experimental XRD patterns. Therefore, the modeling procedure will be described for each model separately. The quality of agreement between the experimental and calculated XRD patterns is estimated by a profile factor R_p (Howard and Preston, 1989):

$$R_p = \left[\frac{\sum_i \left(I_i^{obs} - I_i^{cal} \right)^2}{\sum_i (I_i^{obs})^2} \right]^{1/2}$$

where I_i^{obs} and I_i^{cal} are the measured and calculated intensities at each i step increment.

Thermal gravimetric analysis – mass spectrometry (TGA-MS)

Dehydroxylation reactions *vs.* sample heating were performed on all samples using a TA Instruments model 2050® thermal gravimetric analysis device with a heated capillary tube that was connected to a Thermo Onix quadropole mass spectrometer. All samples were heated at a constant rate of 5ºC/min up to 900ºC. Mass 18 evolved during heating was recorded to represent H_2O from dehydration and dehydroxylation, while mass 44 was recorded and is considered to represent CO_2 from the decomposition of calcite.

Scanning electron microscopy

A Philips model XL-20 scanning electron microscope (SEM) equipped with an EDAX energy-dispersive spectrometer (EDS) was used to obtain magnified images of the studied samples.

SAMPLES

The samples in this study were obtained from percussion sidewall cores, from the ChevronTexaco Alaminos Canyon 815 #1 (AC815 #1) well. The water depth at the well position is ~2800 m. The samples are all from the Upper Oligocene Frio formation. The bottom borehole temperature at AC815 #1 was 42ºC at a depth of 4504 m. Sample depths refer to below sea level. At 3895 m, the temperature was 33ºC and the temperature increased linearly to the bottom of the borehole. These sediments were deposited in a deep-water turbidite system consisting of confined channels and associated sheet-like lobes.

Several studies have been made on the diagenesis, mineralogy, and geochemistry of the Frio Formation sediments from wells on-shore or near-shore, e.g. study by Lynch (1996, 1997) and Bjorlykke (1997) and the citations within. However, few published studies are

available describing the mineralogy from deepwater offshore wells in the Frio Formation.

RESULTS

Whole-rock mineralogy

A summary of the whole-rock mineralogy from the 14 sidewall core samples examined in this study are presented in Table 1. The most significant mineral components are: quartz ranging from 4 to 18% (average 11%); feldspar, 2−14% (average 7%); calcite, 7−56% (average 22%); clinoptilolite, 1−17% (average 10%); and 2:1 layer dioctahedral clay and mica, 26−58% (average 45%). This mineral assemblage suggests a significant volcanic contribution to these Frio Formation sediments. This interpretation is consistent with other published studies of the Frio Formation from on-shore and near-shore locations (*e.g.* Lynch, 1996, 1997; and Bjorlykke, 1997). Rocks from this well were examined extensively by SEM which revealed abundant glass shards (Figure 1) with authigenic clay growing on glass surfaces. In addition to volcanic glass, SEM analysis revealed authigenic zeolite and opaline or cristobalite liposphere consistent with volcanic sediment. The SEM analysis also showed abundant pelagic fossils interpreted to be the main source of calcite in these samples. Other studies have recognized volcanic glass in the Frio Formation of south Texas (Kerr and Grigsby, 1991) and in the deep water of the Gulf of Mexico (Hanan *et al*., 1998).

Samples with abundant clinoptilolite are generally poorer in plagioclase (Table 1). Furthermore, SEM evidence of authigenic clinoptilolite and clay forming in association with glass shards also suggests that unstable plagioclase grains and glass shards may be reacting to form zeolite and clay minerals.

Qualitative description of the experimental XRD patterns

Experimental XRD patterns recorded for 14 oriented EG samples are similar to those characteristic of R0 I-S in which smectite layers prevail ($W_S \geqslant W_I$). These patterns contain intense and well defined 17 Å peaks and a non-rational series of basal reflections. The main difference between the XRD patterns recorded from the different samples is in the migration and profile variation of the basal reflections. Figure 2 shows XRD patterns that demonstrate the diffraction features typical of the sample set. For example, the XRD pattern of sample M496-011 contains a set of basal reflections with *d* values equal to 17.15 Å, 8.62 Å, 5.68 Å, and 3.39 Å. These values deviate only slightly from a rational series. Therefore, this sample should contain a large number of smectite layers. Symmetrical and well resolved from the low 2θ angle side, the 17 Å peak confirms this conclusion. The progression of the XRD patterns corresponding to the sample sequence:

M496-011 → M96-014 → M496-009 → M496-013 → M496-012 → M496-002

consists of the migration of the reflections with *d* values equal to 8.62 Å and 5.68 Å to smaller and larger 2θ angles, respectively, and less well resolved 17 Å peaks at the lower 2θ angle side (Figure 2). According to Mèring's rules, the observed diffraction features are related to increased illite layer content. Note that the samples are numbered from shallow to deep (Table 1).

In XRD patterns from the oriented Mg-saturated AD samples, the positions of the basal reflections are similar to each other. However, there is a difference in the profile and intensity of the basal reflections. For example, for some samples, the reflection at 14.98 Å in the XRD patterns is stronger, narrower, and better

Table 1. Whole-rock mineralogy for the studied samples based on quantitative X-ray phase analysis (wt.%).

Sample	Depth (m)	Quartz	K-feld-spar	Plagio-clase	Calcite	Pyrite	Clinop-tilolite	Kaol-inite	Chlorite	2:1 Clay + mica*	Total
M496-002	4092.85	16	2	7	16	0	3	0	0.9	52	97
M496-003	4093.46	14	2	5	14	0	1	0	0.9	58	96
M496-004	4100.78	4	6	1	50	0	10	0	0	26	97
M496-005	4104.13	5	1	1	56	0	1	0	0	28	96
M496-006	4145.28	7	1	2	36	0	14	0	0.8	38	99
M496-007	4179.42	18	3	2	9	1	16	0	1	48	98
M496-008	4182.47	14	3	3	20	0	13	0	1	42	97
M496-009	4207.46	7	1	0.9	39	0	10	0	0	38	97
M496-010	4209.29	11	2	2	22	0	8	0	0.7	49	95
M496-011	4262.93	14	4	10	11	1	16	0	0.4	39	95
M496-012	4389.43	15	2	8	13	0	14	0	0	48	99
M496-013	4456.18	12	4	6	10	0	17	0	0	48	97
M496-014	4489.09	11	2	2	11	0.5	6	3	0	58	94
M496-015	4499.46	8	2	2	7	0	5	10	2	56	93

* Total 2:1 layer dioctahedral layer silicates, *i.e.* illite, smectite, illite-smectite and mica if present.

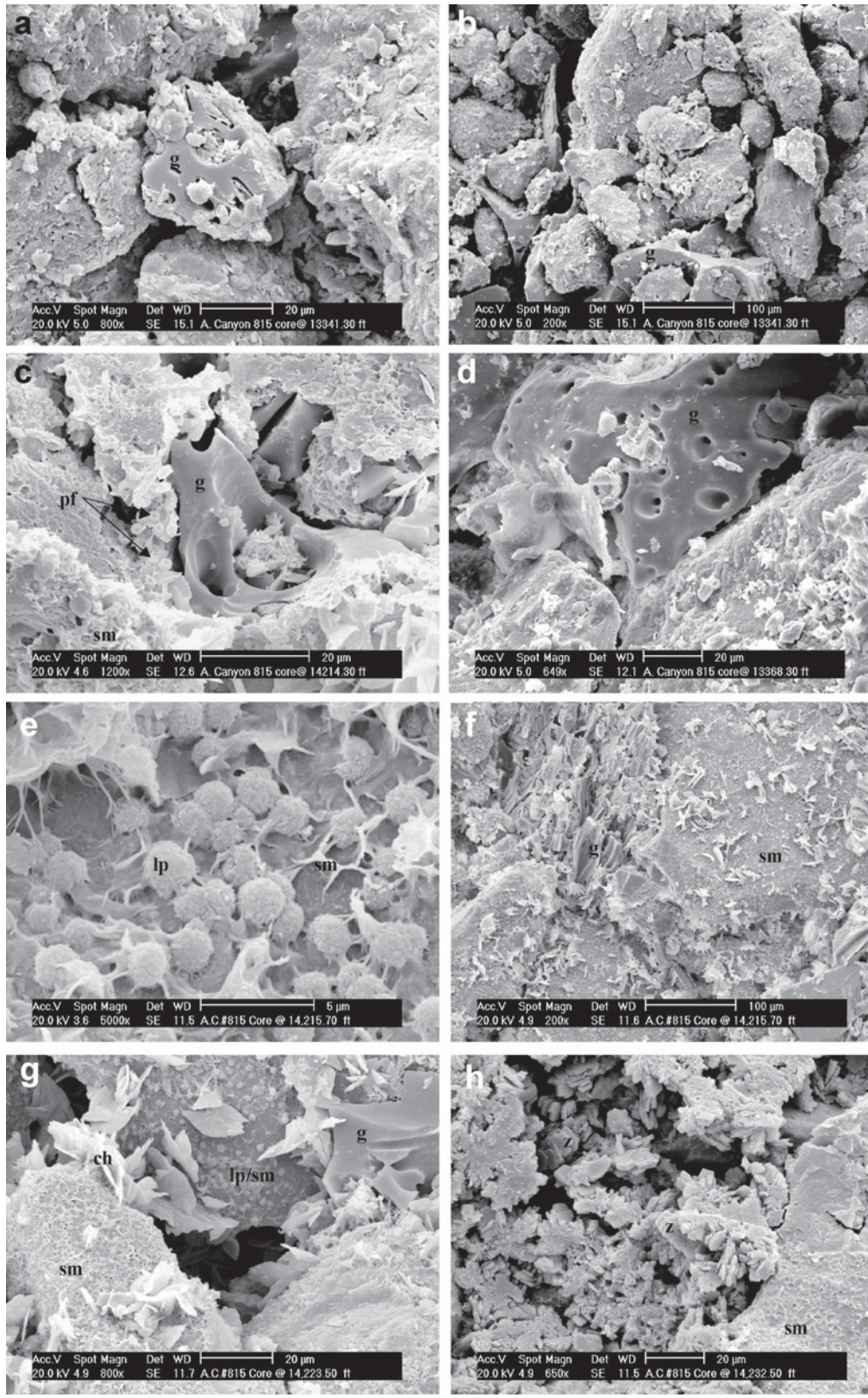

Figure 1. SEM images of samples taken from various depths in the studied well. g = glass, sm = smectite, pf = pelagic fossil, z = zeolite, lp = liposphere, ch = chlorite.

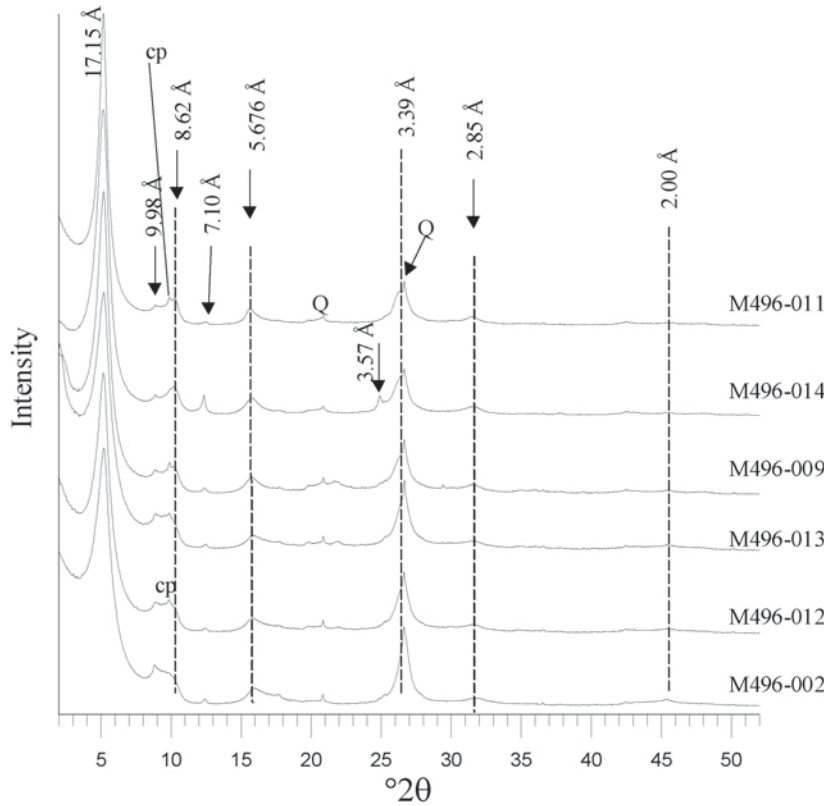

Figure 2. Representative XRD patterns of oriented Ca-saturated specimens after EG solvation comparing greater smectite content (*e.g.* M496-011) progressing to lesser smectite content (*e.g.* M496-002). Q = quartz, cp = clinoptilolite.

resolved on the low-2θ angle side in comparison with other samples.

Quantitative description of the experimental XRD patterns

The multispecimen method was used to simulate the experimental XRD patterns. First, the results of this technique are described for a selected set of XRD patterns representing the typical diffraction features of the whole sample set. These XRD patterns were recorded for samples M496-002, M496-007, M496-009, M496-012, and M496-014, saturated by Mg and Ca in AD and EG states, and the results of the multispecimen method for glycolated and Mg- and Ca-saturated samples were the same. Therefore, for the selected set of samples only results obtained for AD Mg-saturated and EG Ca-saturated specimens are presented to emphasize that, independent of the different states and interlayer exchange cation, the same structural model can be used. The three models that were tested, R0 I-S, segregated I-S, and smectite + R0 I-S mixture, are presented below.

Single-phase R0 I-S model. Because the diffraction features of the experimental XRD patterns recorded for the EG samples are similar to those corresponding to R0 I-S, the method of Środoń (1981) was used to estimate the number of smectite layers in the I-S, taking into account swelling layer thickness and layer thickness distribution in CSDs of the I-S without using the correction for the presence of discrete illite (J. Środoń, pers. comm.). Table 2 contains the expandability values

Table 2. Expandability (W_{exp}) determined by the Środoń (1981) method and by computer simulation for the segregated R1 I-S and two-phase mixture models.

Sample	Depth (m)	Środoń	Segregated	Two-phase*
M496-002	4092.85	77	48	52
M496-003	4093.46	70	52	52
M496-004	4100.78	82	66	64
M496-005	4104.13	72	60	62
M496-006	4145.28	68	64	66
M496-007	4179.42	77	75	73
M496-008	4182.47	80	68	73
M496-009	4207.46	80	70	65
M496-010	4209.29	88	70	70
M496-011	4262.93	95	70	65
M496-012	4389.43	77	60	56
M496-013	4456.18	74	57	55
M496-014	4489.09	80	68	69
M496-015	4499.46	77	75	81

* Expandability for the two-phase mixture is determined as a weight average smectite layer content (%).

which were determined using the peak positions measured from the experimental EG XRD patterns. These data obtained for each EG sample were used to calculate an XRD pattern and to compare it with the experimental one. For the same AD sample, such a comparison was carried out for an R0 I-S model in which the total amount of expandable layers was not changed, but the ratio of the layers containing one and two layers of H_2O molecules in their interlayers was varied to get the best possible agreement between the compared scans (Table 3). Figures 3 and 4 compare the experimental and calculated XRD patterns. The amounts of expandable layers in the R0 I-S are equal to 77% for the M496-002, -007, and -012 samples, and to 80% for the M496-009 and M496-014 samples. The degree of conformity, however, was different for different samples. The values of R_p vary from 14.4% to 26.5% for the AD scans and from 9.9% to 21.9% for EG XRD scans (Table 3). These data, along with the visual comparison of the experimental and calculated XRD patterns, show that the R0 I-S models fail to describe with the same quality the positions, intensities, and profiles of all the reflections observed in the AD and EG XRD patterns.

Single-phase segregated I-S model. To simulate the experimental XRD patterns, a set of trial-and-error steps was used to get a satisfactory agreement between the XRD patterns for each sample in both AD and EG states in terms of the same structural model. This model should have the same amount of illite and expandable layers and the same degree of segregation of the layer types. The number of S_1 and S_2 expandable layers may be different in the AD and EG states but their total numbers should be the same. The experimental and calculated XRD patterns as well as the structural and probability parameters used for the XRD pattern simulation are shown in Figures 5 and 6 and in Table 4. Along with I-S, the samples contain 1−4% of illite material with 5% expandable layers and 1−5% kaolinite (Table 5). The number of illite layers in the I-S varies for different samples from 52% to 25% (Table 4). After EG solvation, the expandable layers in the I-S phases swell to 16.90−17.0 Å and, in sample M496-002, the EG I-S contains 46% of 16.90 Å (2EG) and 2% of 12.90 Å (1EG) layers. In contrast, the I-S in the AD state has two types of expandable layers with different thicknesses (Table 4). The coexistence of layers exhibiting contrasting hydration states within CSDs can be considered as evidence of heterogeneity in the distribution of the layer charge. The values of R_p vary from 7% to 9.1% for EG and from 10.2% to 14.8% for AD XRD patterns (Table 4).

The characteristic feature of the XRD patterns of these samples is that the positions, intensities, and profiles of the basal reflections differ substantially from those corresponding to R0 I-S. For the I-S models $W_j < P_{jj}$, *i.e.* the illite and smectite layers in these structures are distributed with a tendency to segregation (Table 4). The degree of segregation of the layer types may be estimated by the equation (Drits and Tchoubar, 1990):

$$S_g = (P_{jj} - W_j)/(1 - W_j) \quad (1)$$

where W_j is the content of layer type j and P_{jj} is the junction probability for layer type j follows layer type j (j = S or I). To estimate the degree of segregation in the I-S studied, it is convenient to use the illite layer parameters, W_I and P_{II}, in order to ignore the mutual distribution of different expandable layers in the AD I-S. The calculated S_g values are 0.33−0.34 for samples M496-002, M496-012, and M496-014, in which the number of illite layers in the I-S varies from 52% to 32%; the S_g value decreases to 0.27−0.29 for the I-S in samples M496-007 and M496-009, containing 25% and 30% of illite layers (Table 4).

Table 3. Structural and probability parameters obtained for the R0 I-S, and content (wt.%) of discrete illite and kaolinite.

Sample and treatment		h_I	h_{S_1}	h_{S_2}	W_I	W_{S_1}	W_{S_2}	N	R_p	Illite	Kaolinite
M496-002	EG	9.98	16.88		0.23	0.77		6.0	21.9	3	1
	AD	9.98	14.80	13.50	0.23	0.60	0.17	4.0	26.5	3	1
M496-007	EG	9.98	16.96		0.23	0.77		6.0	10.8	3	5
	AD	9.98	14.80	13.50	0.23	0.65	0.12	4.3	17.8	2	5
M496-009	EG	9.98	16.99		0.20	0.80		6.0	13.3	2	1
	AD	9.98	14.90	13.50	0.20	0.65	0.15	4.5	18.9	2	1
M496-012	EG	9.98	16.96		0.23	0.77		6.0	17.3	2	1
	AD	9.98	14.80	13.50	0.23	0.55	0.25	4.5	26.2	2	1
M496-014	EG	9.98	16.99		0.20	0.80		5.0	9.9	2	5
	AD	9.98	14.80	13.20	0.20	0.60	0.20	4.5	14.4	2	5

h_I, h_{S_1}, h_{S_2} are the thicknesses of illite and expandable layers, S_1 corresponds to 2EG and 2W, S_2 to 1EG and 1W expandable layers, respectively.
W_I, W_{S_1}, W_{S_2} are the contents of the I, S_1 and S_2 layers, respectively.
N is the mean number of layers in CSDs
R_p is the profile factor characterizing the overall fit quality

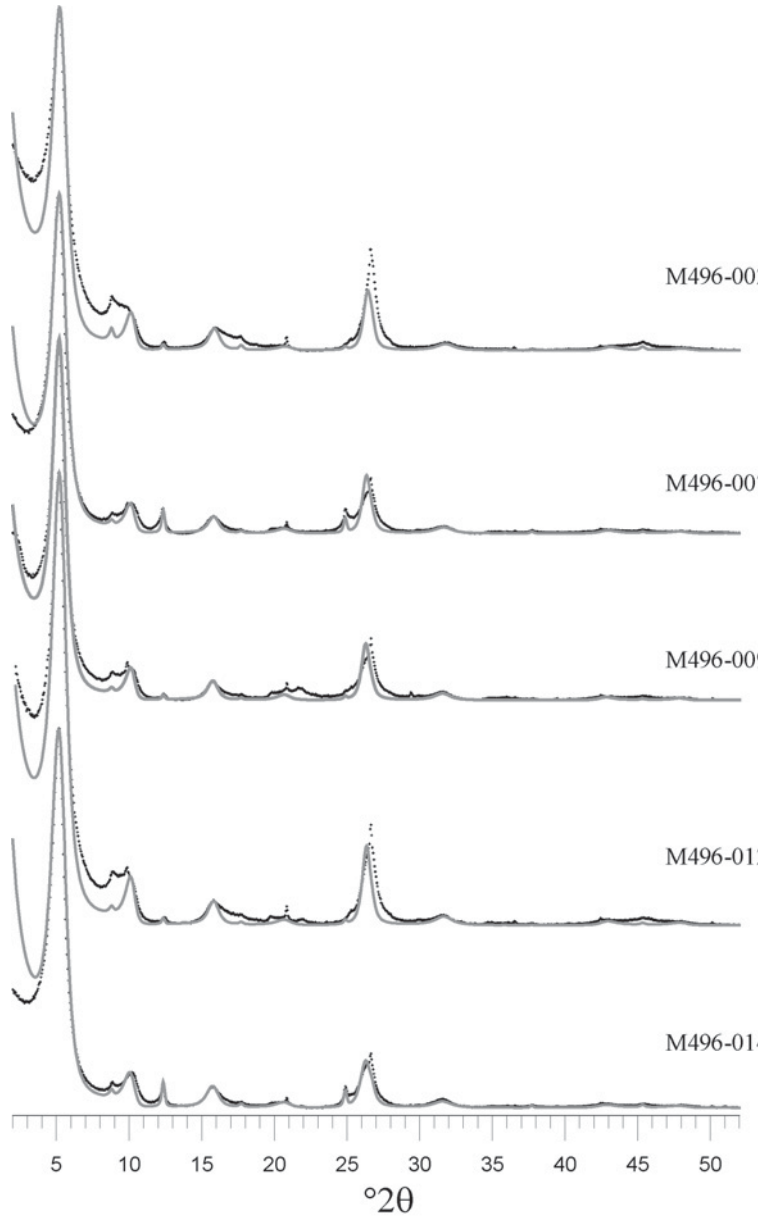

Figure 3. Comparison of the experimental XRD patterns from Ca-saturated and EG-solvated specimens with those calculated (gray curves) for the single R0 I-S model using the illite and smectite layer content and the swelling layer thickness determined by the Środoń (1981) peak-position method.

Two-phase model. This model assumes that each sample contains a physical mixture of pure smectite and R0 I-S. As in the previous model, trial-and-error steps were used to get a satisfactory agreement between the experimental and calculated patterns for each sample in both AD and EG states in terms of the same model. To be valid, the model should contain the same amount of pure smectite and R0 I-S for both EG and AD states. The experimental and simulated XRD patterns are shown in Figures 7 and 8. Table 6 contains the structural and probability parameters for the smectite and R0 I-S, whereas Table 7 contains weight concentrations of the phases which, along with smectite and R0 I-S, were determined for the samples. The primary requirement of the multispecimen analysis is fulfilled and the amount of the main phases determined by simulation of the XRD patterns for each sample in the AD and EG states is almost the same. Table 7 shows that, along with smectite and I-S, the samples contain 1−4% of illitic material with 5−10% of expandable layers and 1−6% of kaolinite. Note especially that the pure smectite content varies irregularly with depth from 28 to 58% (Table 7). A remarkable result is that in all the samples, the I-S contains the same amount of illite and expandable layers, 65% and 35%, respectively. The values of the R_p

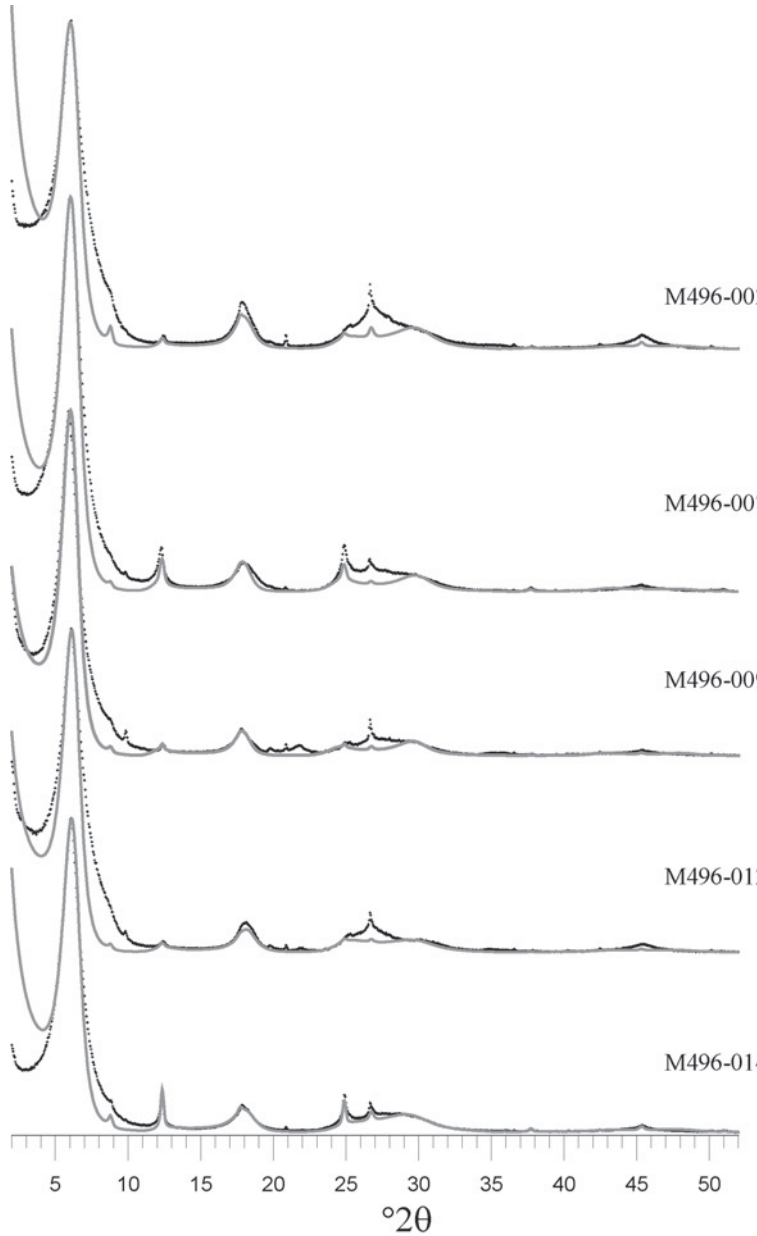

Figure 4. Comparison of the experimental XRD patterns from Mg-saturated AD specimens with those calculated (gray curves) for the single R0 I-S model using the illite and smectite layer content determined by the multi-specimen method.

factors vary from 4.3% to 7.5% for EG and from 6.1% to 10.4% for AD XRD patterns (Table 6). As a rule, for the same sample, the value of the R_p factor determined for the EG-solvated specimen is smaller than that for the AD specimen. This difference is probably related to the fact that the experimental EG XRD patterns were usually described using only one type of expandable layer with well defined thickness and interlayer scattering power. In contrast, to describe AD XRD patterns, two expandable layer types were required for each of them; the thickness and scattering power are variable. Even these small variations have a significant influence on the intensity distribution.

In AD conditions, the R0 I-S consists of 14.60–14.70 Å (2W) and 12.8–13.0 Å (1W) expandable layers containing two and one layers of H_2O molecules in their interlayers, respectively. However, after EG solvation, all these layers swell to 16.85–16.95 Å (2EG), and only 3% of 12.90 Å (1EG) layers are modeled in the I-S of samples M496-002, M496-009, and M496-013. The pure smectite in the AD state also consists of 14.70–14.75 Å and 12.8–13.0 Å layers, among which the first layer type prevails (Table 6). In addition, two smectite varieties coexist in samples M496-012 and M496-014. One of them contains both 14.75 Å and 12.8–13.0 Å layers whereas the other

Table 4. Structural and probability parameters obtained for the segregated R1 I-S.

Sample and treatment		h_I	h_{S_1}	h_{S_2}	W_I	W_{S_1}	W_{S_2}	P_{II}	P_{IS_1}	P_{IS_2}	P_{S_1I}	$P_{S_1S_1}$	$P_{S_1S_2}$	P_{S_2I}	$P_{S_2S_1}$	$P_{S_2S_2}$	N	S_g	R_p
M496-002	EG	9.98	16.90	12.90	0.52	0.46	0.02	0.679	0.318	0.002	0.34	0.62	0.04	0.52	0.46	0.02	9.0	0.33	8.7
	AD	9.98	14.80	13.20	0.52	0.36	0.12	0.679	0.201	0.120	0.38	0.50	0.12	0.25	0.63	0.12	6.0		10.2
M496-007	EG	9.98	16.95		0.25	0.75		0.45	0.55		0.183	0.817					4.0	0.27	7.0
	AD	9.98	14.80	13.40	0.25	0.50	0.25	0.45	0.30	0.25	0.15	0.60	0.25	0.25	0.50	0.25	4.0		14.4
M496-009	EG	9.98	16.95		0.30	0.70		0.50	0.50		0.214	0.786					5.0	0.29	9.1
	AD	9.98	14.90	13.50	0.30	0.55	0.15	0.50	0.35	0.15	0.191	0.659	0.15	0.30	0.55	0.15	4.5		14.1
M496-012	EG	9.98	16.90		0.40	0.60		0.60	0.40		0.267	0.733					5.5	0.33	8.6
	AD	9.98	14.60	13.20	0.40	0.45	0.15	0.60	0.25	0.15	0.222	0.628	0.15	0.40	0.45	0.15	5.0		14.8
M496-014	EG	9.98	17.00		0.32	0.68		0.55	0.45		0.212	0.788					6.0	0.34	8.1
	AD	9.98	14.80	13.20	0.32	0.50	0.18	0.55	0.45	0.00	0.173	0.532	0.295	0.32	0.50	0.18	5.0		11.6

h_I, h_{S_1}, h_{S_2} are the thicknesses of illite and expandable layers, S_1 corresponds to 2EG and 2W, S_2 to 1EG and 1W expandable layers, respectively
W_I, W_{S_1}, W_{S_2} are contents of the I, S_1 and S_2 layers, respectively.
N is the mean number of layers in the CSDs.
S_g is the segregation parameter.
R_p is the profile factor characterizing the overall fit quality.

consists of 14.2 Å layers only. The amounts of the first and second smectite varieties are 22% and 12% for sample M496-012 and 42% and 8% for sample M496-014, respectively (Table 7.) Similar to the R0 I-S, after EG solvation all layers in both smectite varieties expand to 16.80−16.95 Å. Only the smectite phase in sample M496-007, along with 95% of 16.95 Å layers, contains 5% of 12.9 Å layers (Table 6).

Simulation of the XRD patterns for EG specimens of the rest of the samples. Simulation of the rest of the EG XRD patterns using both the two-phase and segregation models confirmed the conclusions made for the selected sample set. In all samples, the I-S phase contains 65% of 9.98 Å illite layers and 35% of smectite layers with random interstratification independent of depth. Table 8 contains the weight concentrations of pure smectite and R0 I-S as a function of depth. The amount of illite and smectite layers in the segregated I-S model, as well as the weight concentration of illite and kaolinite determined by the EG XRD pattern simulation of the rest of the samples are also given in Table 8. Note that for each sample, the R_p value determined for the segregated model is significantly greater (except sample M496-015) than that determined for the two-phase model (Table 8).

Relationships between the probability parameters determined for the AD and EG I-S models

Using the AD and EG models, the values of the W_j and P_{ij} parameters for the I-S structures of the same samples are different (Tables 4 and 6). The reason is that the AD I-S phases, as a rule, contain two types of smectite layers, 1W and 2W, having different thicknesses, whereas, in the EG I-S structures most of the expandable layers swell homogeneously to 2EG. As a result, the values of the W_j and P_{ij} parameters are also different (Tables 4 and 6). However, the distribution of illite and expandable layers in the I-S should be identical in both states. Therefore, the three-component system of the AD I-S must be reduced to the two-component system in the EG states if 1W and 2W layers are

Table 5. Phase composition of the samples determined using the segregated model (wt.%).

Sample and treatment		I-S	Illite	Kaolinite
M496-002	EG	95	4	1
	AD	98	1	1
M496-007	EG	93	2	5
	AD	93	2	5
M496-009	EG	98	1	1
	AD	98	1	1
M496-012	EG	97	2	1
	AD	97	2	1
M496-014	EG	95	1	4
	AD	94	1	5

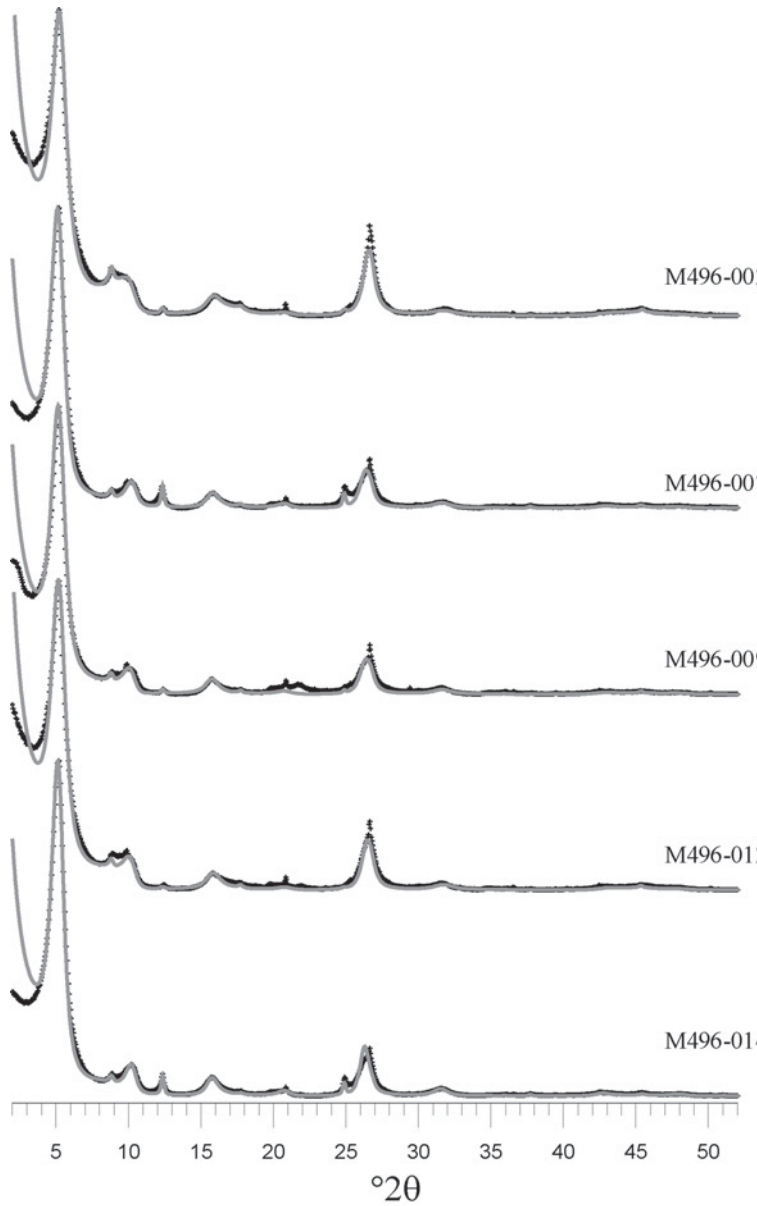

Figure 5. Experimental and simulated XRD patterns for representative Ca-saturated and EG-solvated samples based on the segregated R1 I-S model.

replaced by 2EG layers. For example, let us consider R0 I-S in which W_I of illite layers are interstratified with W_{S_1} of 14.70 Å (2W) and of 12.80 Å (1W) smectite S_1 and S_2 layers, respectively. If in the EG I-S samples, all the smectite layers swell to 16.90 Å, then the following relationships should be valid:

$$W_{SI} = W_{S_1I} + W_{S_2I} \quad (2)$$
$$W_{IS} = W_{IS_1} + W_{IS_2} \quad (3)$$
$$W_{SS} = W_{S_1S_1} + W_{S_1S_2} + W_{S_2S_1} + W_{S_2S_2} \quad (4)$$

Here, W_{ij} is the occurrence probability for an ij layer pair and i,j = I, S_1, S_2 for the AD three-component and i,j = I, S for the EG two-component I-S, respectively.

For R0 I-S the validity of these equations is obvious because $W_{ij} = W_iW_j$ and the values of W_I, W_{S_1}, W_{S_2}, and W_S are known for EG and AD specimens of each sample (Table 6). The relationships (2−4) should also be valid for the AD three-component and EG two-component segregated I-S (Table 4). However, in this case, $W_{ij} = W_iP_{ij}$ because for these structures R = 1. The values of the W_{ij} parameters for the segregated I-S in the AD and EG states (sample M496-009) are shown by the matrix in Table 9. Each W_{ij} value in the matrix is located at the interaction of i^{th} row and j^{th} column. For example, using Table 4, one can calculate the W_{IS_1} value for the AD I-S $W_{IS_1} = W_IP_{IS_1} = 0.3 \times 0.35 = 0.105$. In the matrix, this

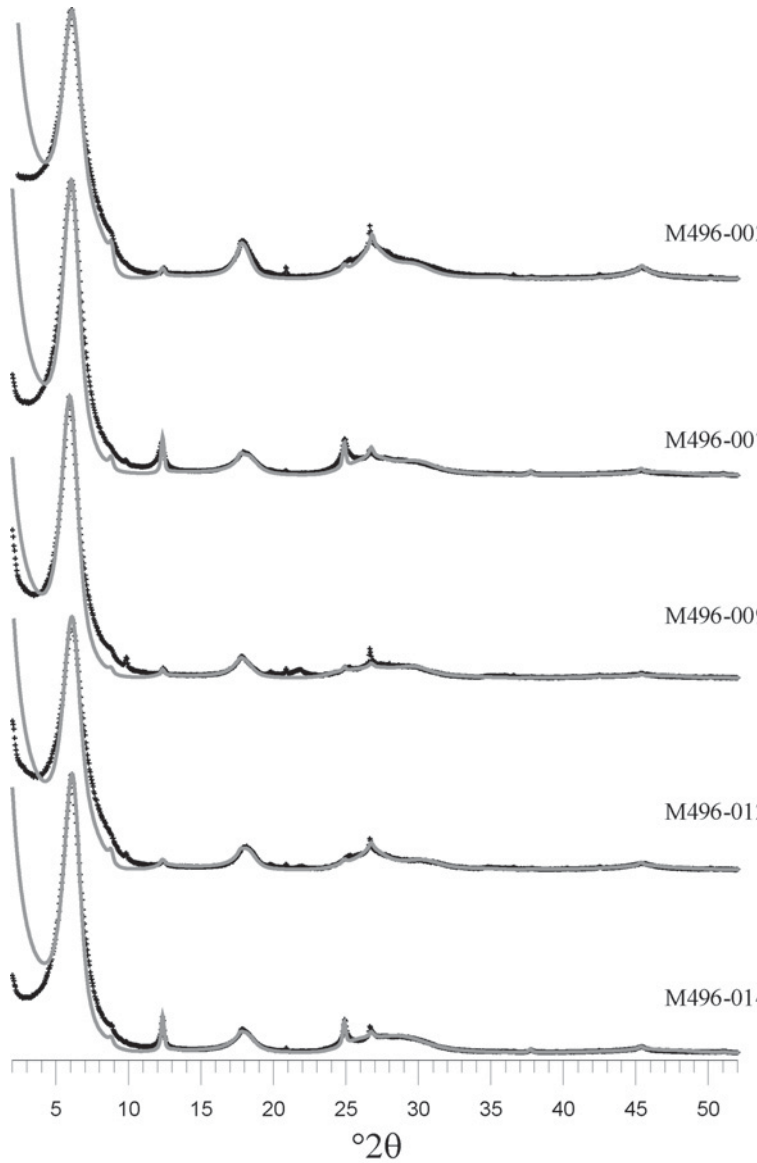

Figure 6. Experimental and simulated XRD patterns for representative Mg-saturated, AD samples, based on the segregated R1 I-S model.

value stands at the intersection of I^{th} row and S_I^{th}column. As was shown above, the W_{ij} values obtained for AD and EG states should be related by the relationships (2−4). Comparison of the W_{ij} values given in the darker boxes in the matrix for AD and EG I-S confirms the validity of these relationships. Similar relationships can be considered for each I-S phase in each sample.

Thermal effects

The DTG curves of all samples (not shown) contain two main endothermic peaks at 100−105ºC and 400−450ºC related to dehydration and dehydroxylation, respectively. Drits *et al*. (1995, 1998) showed that the dehydroxylation temperature of dioctahedral Al-rich 2:1 layers depends on the distribution of octahedral cations between *trans*- and *cis*-sites. A DTG peak of <600ºC indicates *trans*-vacant (*tv*) layers, and *cis*-vacant (*cv*) layers when DTG peaks are >600ºC. The dehydroxylation temperatures in all samples show that the 2:1 layers have *tv* octahedra. The TGA-MS analysis was also used to confirm the presence of calcite and kaolinite observed in XRD scans. Figure 9a from sample M496-004 shows the thermal data, weight loss, and corresponding evolved gas from mass 44 representing CO_2, resulting from the decomposition of calcite, based on the mass 44 peak at ~721ºC. The greater area under the dehydroxylation peak at 500ºC observed for sample M496-015 (Figure 9b) compared to the other samples can be

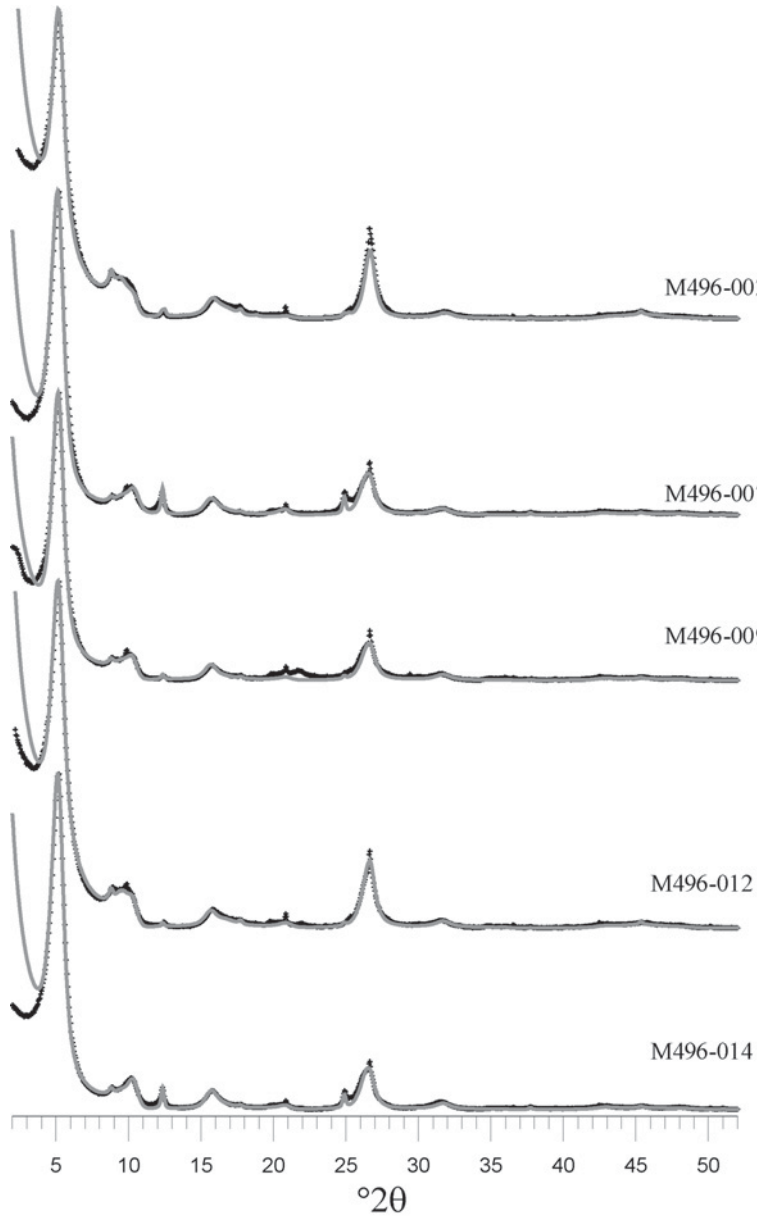

Figure 7. Experimental and simulated XRD patterns for representative Ca-saturated and EG-solvated samples based on the R0 I-S and discrete smectite two-phase model.

considered as indirect evidence of significant kaolinite content. Kaolinite was also identified qualitatively by Fourier transform infrared spectroscopy (not shown).

DISCUSSION

Choice of model, and mineralogical evidence

In general, the results of this work show that the two-phase and segregated I-S models can describe the experimental XRD patterns recorded in EG and AD states significantly better than the single R0 I-S model. However, the two-phase model has consistently smaller R_p factors than does the segregated model (Tables 4, 6, 8) thus indicating that it is more reliable. To verify and have independent evidence for this model, other criteria were considered to decide which of these models corresponds to the actual structure. To make a choice, consider the evolution of structural and probability parameters of the segregated I-S phases with depth. Figure 10 shows that the expandability of the segregated I-S varies from 48% to 75% without any relationship between the number of smectite layers and depth. Such an irregular variation of 'smectite illitization', based on the segregation model, does not have a rational explanation considering the relatively narrow stratigraphic interval (~427 m) and low temperature, even at

Table 6. Structural and probability parameters of smectite and R0 I-S determined for the two-phase model.

Sample and treatment		Smectite					Illite-smectite					R_p
		h_{S_1}	h_{S_2}	W_{S_1}	W_{S_2}	N	h_{S_1}	h_{S_2}	W_{S_1}	W_{S_2}	N	
M496-002	EG	16.80	–	1	0	4.0	16.95	12.90	0.32	0.03	7.0	6.7
	AD	14.70	13.00	0.75	0.25	3.8	14.70	13.00	0.25	0.10	12.0	7.3
M496-007	EG	16.95	12.90	0.95	0.05	4.0	16.85	–	0.35	0	7.0	7.5
	AD	14.75	12.80	0.65	0.35	3.3	14.70	12.80	0.25	0.10	12.0	6.5
M496-009	EG	16.90	–	1	0	4.0	16.90	12.90	0.32	0.03	7.0	7.3
	AD	14.75	13.00	0.75	0.25	3.3	14.70	12.80	0.23	0.12	12.0	8.6
M496-012	EG	16.90	–	1	0	4.0	16.90	–	0.35	0	8.0	4.3
	AD	14.75	12.80	0.75	0.25	3.5	14.60	13.00	0.22	0.13	15.0	9.3
M496-013	EG	16.90	–	1	0	4.0	16.95	–	0.32	0.03	8.0	6.0
	AD	14.70	13.00	0.65	0.35	3.3	14.70	13.00	0.30	0.05	12.0	10.4
M496-014	EG	16.90	–	1	0	4.0	16.95	–	0.35	0	7.0	5.2
	AD	14.75	13.00	0.60	0.40		14.70	13.00	0.25	0.10	12.0	6.1

h_{S_1}, h_{S_2} are the thicknesses of expandable layers S_1 and S_2, respectively; the notation for S_1 and S_2 is given in Table 3.
W_{S_1}, W_{S_2} refer to relative contents of S_1 and S_2 layers.
N is the mean number of layers in the CSDs .
R_p is the profile factor characterizing the overall fit quality.

the bottom of the well (42ºC). Any significant diagenetic transformation of I-S under such conditions is unlikely.

To explain such an erratic I-S expandability profile with depth, specific geological processes would have to have occurred: (1) either detrital I-S with different expandabilities would have had to be deposited at different times in the 427 m section, contrary to I-S in the present Mississippi river system (*e.g.* Hoffman, 1979); or (2) different geochemical processes affected the individual samples, such as elevated K in the pore fluids (*e.g* Huang *et al*., 1993), that could, perhaps, have resulted from different permeability. Mercury injection porosimetry analysis shows that porosity is relatively constant in these samples, 19−25%. Thus, in a buffered marine environment, significant differences in K content in the pore fluids of these samples is difficult to imagine. No evidence exists that shows any of the samples were located in a hydraulically isolated or independent zone by impermeable baffles or barriers.

In contrast, the main features of the phase composition of the samples determined using the two-phase model are consistent with the mineralogical association of the Frio Formation and its volcanic components. Therefore, one naturally assumes that the association of pure smectite and R0 I-S is related to their different origins considering the classic model of the progressive illitization of smectite and the low maximum burial temperature of 42ºC in this section. A detrital origin for the R0 I-S is in agreement with the large number of illite layers in the I-S structure (65%), and that is unchanged with depth. R0 I-S with an illite layer proportion of ~65% has been reported in ancient rocks (*e.g.* Claret *et al*., 2004), soils (Righi *et al.*, 1995; Velde and Peck, 2002), and paleosols (Huggett and Cuadros, 2005). However, it is possible that the I-S is

Table 7. Phase content of the samples determined using the two-phase model (wt.%).

Sample and treatment		I-S	Smectite	Illite	Kaolinite
M496-002	EG	68	28	2	2
	AD	69	28	2	1
M496-007	EG	35	58	2	5
	AD	36	54	4	6
M496-009	EG	48	50	1	1
	AD	51	47	1	1
M496-012	EG	61	36	2	1
	AD	63	34*	2	1
M496-013	EG	67	30	2	1
	AD	62	35	2	1
M496-014	EG	44	51	1	4
	AD	44	50*	1	5

*smectite phase consists of two varieties. In M496-012 it contains 22% smectite (consisting of 14.75 Å and 12.80 Å interstratified layers), and 12% smectite (consisting of 14.2 Å layers only). Sample M496-014 contains 42% of the smectite variety (consisting of 14.75 Å and 13.0 Å interstratified layers), and 8% smectite (consisting of 14.2 Å only).

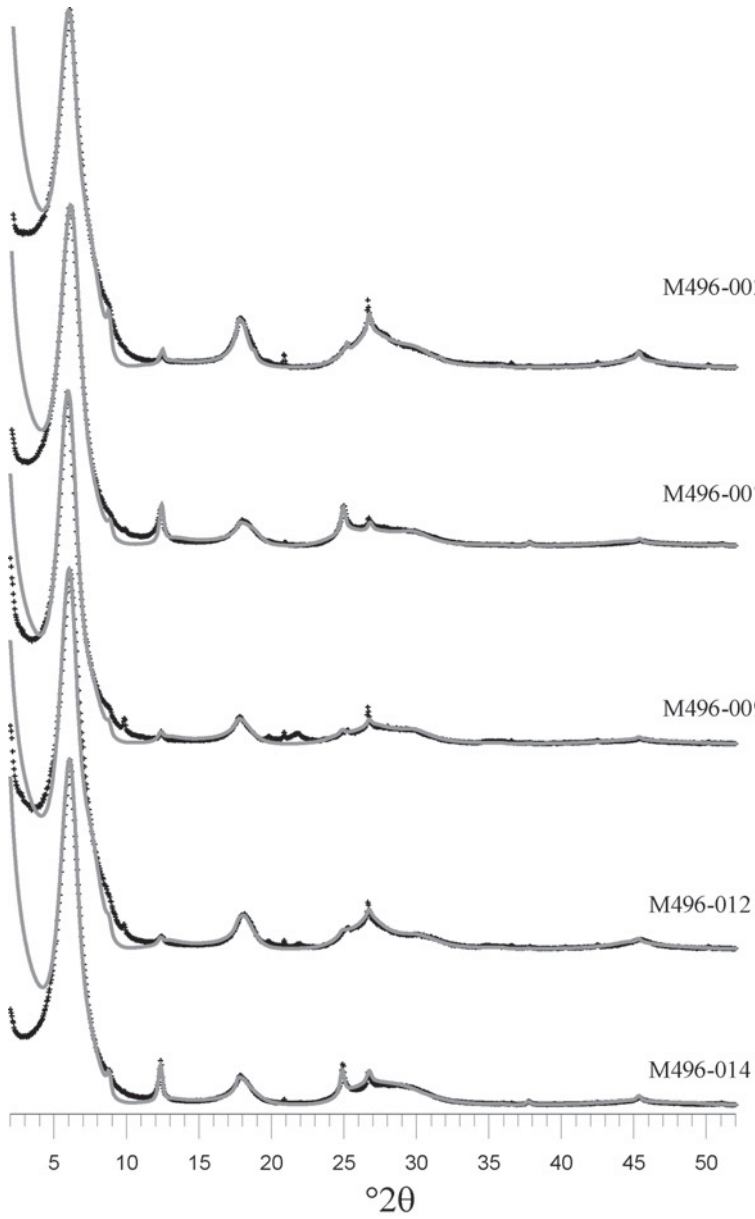

Figure 8. Experimental and simulated XRD patterns for representative Mg-saturated AD samples based on the R0 I-S and discrete smectite two-phase model.

authigenic. If so, there must have been localized variability in the K concentration from K-feldspar dissolution. Unfortunately there is no direct evidence to confirm or reject this possibility.

The SEM images confirm the authigenic origin of smectite (Figure 1). Transformation of volcanic ash and glass into smectite and zeolite is a well known and widespread reaction occurring at low temperature over a wide spectrum of pH, especially in mildly alkaline conditions such as in marine environments (Moore and Reynolds, 1997) and in non-marine formations with abundant volcanic glass (*e.g.* Pevear *et al.*, 1980).

The amount of smectite phase increases from 28% at the top of the Formation at ~4093 m to 56% at 4179−4182 m, then decreases to 30% at 4456 m and increases again to 63% at the bottom of the section (Figure 10). Such an irregular variation of both smectite and clinoptilolite content with depth is probably determined by local variations in the amount of initial volcanic material. Thus, consideration of the particular features of the mineral assemblage and the volcanic component of the studied Frio Formation, in addition to the lower R_p values of the two-phase model, leads to the conclusion that the segregation model must be rejected.

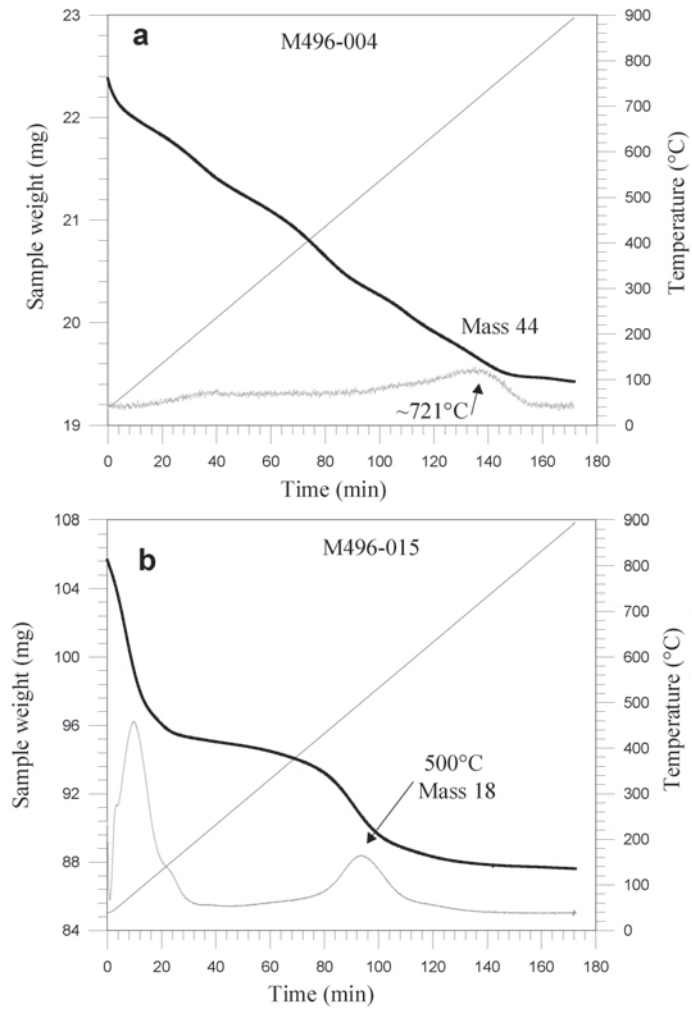

Figure 9. (a) TGA-MS data for sample M496-004. Temperature = straight line, weight loss = dark line, Mass 44 (CO_2) = shaded line (relative intensity). (b) TGA-MS data for sample M496-015. Temperature = straight line, weight loss = dark line, Mass 18 (H_2O) = shaded line (relative intensity).

Table 8. Weight concentration (%) of R0 I-S and smectite in the two-phase mixtures; relative number of the interstratified layers in the segregated R1 I-S; weight concentration of discrete minerals determined for the rest of the samples in the EG state for the two-phase model.

Sample	Depth (m)	Two-phase model I-S	Two-phase model Smectite	R_p	Segregated model W_I	Segregated model W_{S_1}	Segregated model W_{S_2}	S_g	R_p	Discrete minerals Illite	Discrete minerals Kaolinite
M496-003	4093.46	69	28	7.1	0.48	0.48	0.04	0.23	9.2	2	1
M496-004	4100.78	51	46	6.0	0.34	0.64	0.02	0.31	9.0	2	1
M496-005	4104.13	54	42	9.0	0.38	0.58	0.04	0.29	11.9	2	2
M496-006	4145.28	48	49	6.6	0.36	0.60	0.04	0.31	10.5	2	1
M496-008	4182.47	36	56	7.7	0.32	0.64	0.04	0.32	11.4	3	5
M496-010	4209.29	41	55	7.3	0.30	0.68	0.02	0.39	8.5	1	3
M496-011	4262.93	50	48	10.2	0.30	0.68	0.02	0.39	14.5	1	1
M496-013	4456.18	67	30	6.0	0.43	0.54	0.03	0.24	9.3	2	1
M496-015	4499.46	26	63	10.3	0.25	0.71	0.04	0.26	9.3	2	9

The notation for W_I, W_{S_1}, and W_{S_2} is given in Table 3.
S_g is the segregation parameter.
R_p is the profile factor characterizing the overall fit quality.

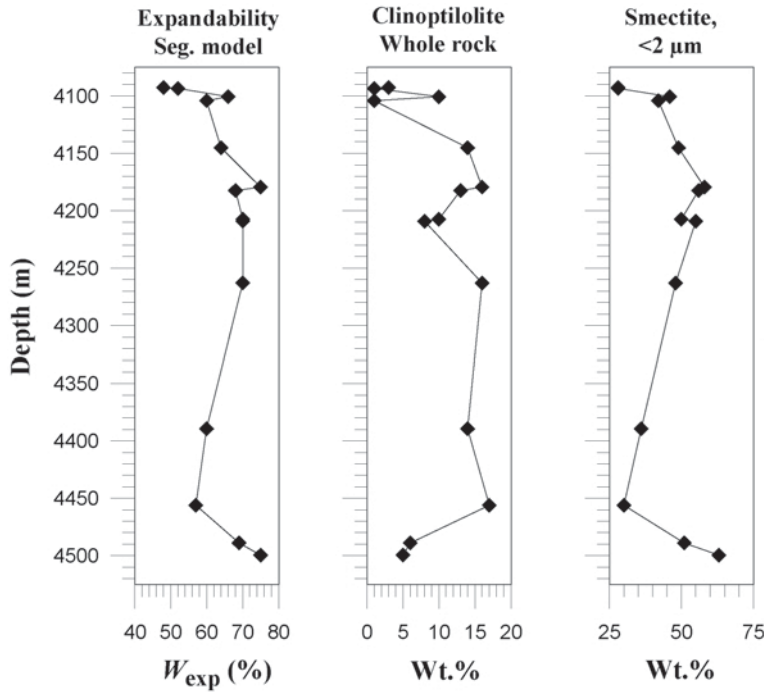

Figure 10. Expandability of the segregated R1 I-S, bulk-rock clinoptilolite concentration and smectite content from the two-phase model (<2 μm fraction).

Expandability determined by different models

Expandability is an important characteristic of clays; of smectite and mixed-layer minerals in particular. The expandability of mixed-layer clay minerals is determined by the number of smectite layers in their structure. Therefore, several convenient techniques have been established to determine the amount of expandable layers in R0 I-S using peak positions and other parameters of the XRD patterns (Środoń, 1981, 1984; Moore and Reynolds, 1997). As was shown, the XRD patterns from the smectite-rich clay samples are visually similar to those from R0 I-S with $W_S \geqslant W_I$, but can be interpreted using either the segregated or two-phase model. The question is how does expandability depend on the chosen model? The expandability of the segregated and R0 I-S is determined by the relative amount of smectite layers. In the case of a physical mixture of pure smectite and R0 I-S, the following procedure is used to determine the relative amount of smectite layers.

Table 9. Relationships between W_{ij} parameters determined for the AD and EG R1 I-S in sample M496-009.

W_i	AD	W_{ij}		
		I	S_1	S_2
0.30	*I*	0.150	0.105	0.045
0.55	S_1	0.105	0.3625	0.0825
0.15	S_2	0.045	0.0825	0.0225

W_i	EG	W_{ij}	
		I	*S*
0.30	*I*	0.150	0.150
0.70	*S*	0.150	0.550

The weight concentrations of coexisting smectite and I-S phases are known for each sample from the experimental XRD pattern modeling (Tables 7, 8). After normalization of these concentrations to 100%, the corresponding concentration values for smectite and I-S are noted as C_S' and $C_{I\text{-}S}$, respectively, and $C_S' + C_{I\text{-}S} = 1$. The weight concentration of smectite layers, C_S'', in the I-S phase can be determined from the equation:

$$\frac{C_S''}{(C_{I\text{-}S} - C_S'')} = \frac{M_S N_S}{M_I N_I} \quad (5a)$$

Here M_S and M_I are the molecular weights of smectite and illite layers and N_S/N_I is the ratio of the smectite and illite layers in the I-S with W_I = 65%, W_S = 35%, and $W_S/W_I = N_S/N_I$; N_S and N_I are the numbers of smectite and illite layers in the mean CSD of the I-S. The total weight concentrations of smectite and illite layers in the mixture are:

$$C_I = C_{I\text{-}S} - C_S'', \; C_S = C_S' + C_S'', \text{ and } C_I + C_S = 1.$$

The molecular weights of glycolated and Ca-saturated expandable layers of pure smectite and of R0 I-S are considered identical.

Therefore:

$$\frac{C_S}{C_I} = \frac{M_S n_S}{M_I n_I} \text{ and } W_{exp} = \frac{n_S}{(n_S + n_I)} = \frac{C_S M_I}{(C_S M_I + C_I M_S)} \quad (5b)$$

Here W_{exp} is the relative amount of smectite layers in the mixture of smectite and R0 I-S of each sample, n_S and n_I are the total number of smectite and illite layers in the coexisting pure smectite + R0 I-S. Equation 5b is obtained by analogy from Equation 5a. Table 2 and Figure 11 compare the expandability values calculated from Equation 5b with those determined for the segregated I-S phases, along with the expandability determined by the Środoń (1981) method. Surprisingly, the expandability determined for the two-phase and segregation models of the same sample coincides within 5%. This means that XRD patterns from a physical mixture of pure smectite and R0 I-S and from a segregated I-S structure are similar or identical if the relative contents of the interstratified layer types in both structure models are also similar. From a diffraction point of view, an addition of a pure smectite to a R0 I-S with W_I = 0.65 and W_S = 0.35 is equivalent to an I-S phase with the same or similar content of smectite and illite layers and with a certain degree of segregation of the interstratified layer types. The factors responsible for the similarity of the XRD patterns from these two different structure models deserve special consideration, but that is beyond the scope of this paper.

The total smectite content in each sample is significantly smaller for most samples than the expandability determined by the Środoń (1981) technique (Table 2, Figure 11). The optimal means of determining the structure and expandability of samples is probably by simulation of the experimental XRD patterns.

Origin of the detrital I-S

A remarkable feature of the I-S in these samples is that the illite-smectite layer ratio of 65%I−35%S does not change within a depth interval of ~427 m and the layers are randomly interstratified. This differs from those described in most classic studies on Gulf Coast sediments (*e.g.* Perry and Hower, 1970; Hower *et al*., 1976; Moore and Reynolds, 1997), where layer stacking usually changed to R1 when the illite layer content was ~55−65%. One possible reason is that in these studies the clay fractions of these sediments were assumed usually to consist of homogeneous I-S with $W_S > W_I$, whereas the actual phase composition of the clay fraction is a physical mixture of pure smectite and R0 I-S. This assumption is in agreement with recent results obtained by Claret *et al*. (2004), Lanson *et al.* (2005), McCarty (2005), Aplin *et al*. (2006), and TEM observations (Dong, 2005). The present-day temperature of 40ºC appears to be the maximum temperature in this section, and is consistent with a detrital origin of the I-S. The detrital I-S in these samples may have retained the structure and expandability in the host rock from which it eroded, *e.g.* the Mesozoic shale formation sources supplying sediment to the Missouri River (Hoffman, 1979). If this phase is authigenic, it may imply that the I-S structure with 65% illite layers is stable at a lower temperature than is usually thought for I-S in this type of marine formation.

The bulk of the Frio Formation sediment in this section was deposited in deep water after transportation

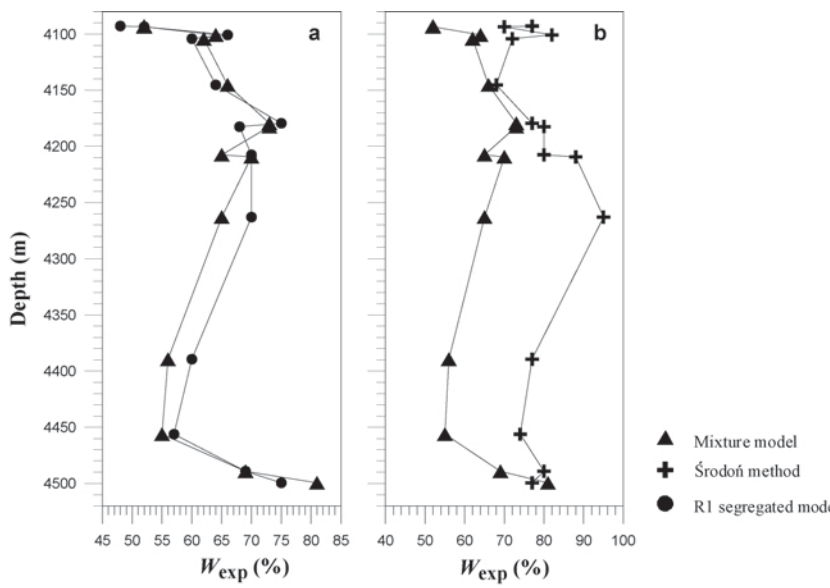

Figure 11. Comparison of expandabilities determined for the segregated R1 I-S and the mixtures of smectite and R0 I-S (a) and expandibilities from the Środoń (1981) method, and from the two-phase mixtures determined as the weighted average smectite layer content (b).

in turbidity flows (Chevron internal report) that are known to occur after submarine avalanches from the unstable Mississippi River delta. Prior to deposition in the delta, a large volume of the sediment would have been subjected to similar physical conditions when transported hundreds of kilometers in the fluvial system over perhaps hundreds or thousands of years. Perhaps the physical and chemical conditions during transport to the basin influenced the character of the observed R0 I-S with W_I ~65% in some unknown way.

Alternatively, deposition of a 427 m section of sediment in the deepwater having had exactly the same transport history in the fluvial system may not be reasonable. R0 I-S with an illite layer content of ~65% illite layers has been reported in the Paris Basin over a thick stratigraphic section (*e.g*. Claret *et al*., 2004) and in Gulf Coast shales (Lanson *et al*., 2005). Thus, perhaps another mechanistic explanation is involved and the I-S layer ratio for random interstratification is limited. Perhaps R0 I-S with a ~65% illite layer content is stable or metastable over a broad range of physical conditions; or more so than other I-S structures. More work is required to understand the exact evolution of this phase and to answer, among other questions, whether the I-S comes from erosion of older formations and, if so, did any processes occur during transport that significantly altered the I-S structure? Investigations of the I-S in the Mesozoic mudstones that contribute sediment to the Gulf of Mexico basin and the I-S in the present day Mississippi river and flood plains, using comparable methods and findings as in this study, may provide further insights.

CONCLUSIONS

The results of the simulation of the experimental XRD patterns recorded for air-dried and ethylene-glycolated samples from the Upper Oligocene Frio formation lead to the following conclusions.

(1) Despite a visual similarity of the experimental XRD patterns to those from R0 I-S in which $W_S \geqslant W_I$, the application of the multispecimen method showed that the actual structure of the studied samples can be described using two different models, both of which differ dramatically from R0 I-S structures. However, the two-phase model is preferable because it provides significantly smaller R_p factor values compared with those determined for the segregation model.

(2) The actual structure of the studied samples is a physical mixture of pure authigenic smectite and an R0 I-S with 65% illite layers. At low temperatures, most of the diagenetically transformed clays probably consist not of a single I-S, but of physical mixtures of smectite and I-S. This conclusion is in agreement with the latest results of Claret *et al*. (2004), Lanson *et al*. (2005), Aplin *et al*. (2006), and numerous TEM investigations (Dong, 2005). The origin of the I-S in these particular rocks is probably detrital.

(3) Pure bentonites may contain a single R0 I-S and in this case conventional methods for determination of the expandability in R0 I-S based on peak position approaches should work perfectly well, whereas for the clay fraction of most sedimentary rocks, modeling of their XRD patterns is necessary. A special investigation is needed to check the validity of this assumption.

ACKNOWLEDGMENTS

The authors gratefully acknowledge Chevron, Inc., and its partners for supporting this work. We also thank Edwin Zeelmaekers for his help and critical review of the manuscript. VAD and BAS thank the Russian Foundation for Basic Research. The review committee, Associate Editor, B. Lanson, and reviewers D. Pevear, and J. Środoń deserve special thanks for their careful reviews and constructive criticisms that significantly improved the paper.

REFERENCES

Altaner, S.P. and Ylagan, R.F. (1997) Comparison of structural models of mixed-layer illite/smectite and reaction mechanisms of smectite illitization. *Clays and Clay Minerals*, **45**, 517–533.

Aplin, A.C., Matenaar, I.F., McCarty, D.K., and van Der Pluijm, B.A. (2006) Influence of mechanical compaction and clay mineral diagenesis on the microfabric and pore-scale properties of deep-water Gulf of Mexico Mudstones. *Clays and Clay Minerals*, **54**, 500–514.

Bjørlykke, K. (1997) Mineral/water interaction, fluid flow, and Frio sandstone diagenesis: evidence from the rocks: discussion. *American Association of Petroleum Geologists Bulletin*, **81**, 1534–1535.

Burst, J.F. (1969) Diagenesis of gulf coast clayey sediments and its possible relation to petroleum migration. *American Association of Petroleum Geologists Bulletin*, **53**, 73–93.

Claret, F., Sakharov, B.A., Drits, V.A., Velde, B., Meunier, A., Griffault, L., and Lanson, B. (2004) Clay minerals in the Meuse-Haute Marne underground laboratory (France): Possible influence of organic matter on clay mineral evolution. *Clays and Clay Minerals*, **53**, 515–532.

Dong, H. (2005) Interstratified illite-smectite: A review of contributions of TEM data to crystal chemical relations and reaction mechanisms. *Clay Science, 12, Supplement 1*, 6–12.

Drits, V.A. (1987) Mixed-layer minerals: Diffraction methods and structural features. *Proceedings of the International Clay Conference, Denver, 1985* (L.G. Schultz, H. van Olphen, and F.A. Mumpton, editors). The Clay Minerals Society, Bloomington, Indiana, pp. 33–45.

Drits, V.A. (1997) Mixed-layer minerals. Pp. 153–190 in: *Modular Aspects of Minerals* (S. Merlino, editor). EMU Notes in Mineralogy, **1**. Eötvös University Press, Budapest.

Drits, V.A. (2003) Structural and chemical heterogeneity of clay minerals. *Clay Minerals*, **38**, 403–432

Drits, V.A. and Sakharov, B.A. (1976) *X-ray Analysis of Mixed-layer Clay Minerals*. Nauka, Moscow, 256 pp. (in Russian).

Drits, V.A. and Tchoubar, C. (1990) *X-ray Diffraction by Disordered Lamellar Structures*. Springer-Verlag, Berlin, 371 pp.

Drits, V.A., Besson, G., and Muller, F. (1995) Structural mechanism of dehydroxylation of cis-vacant 2:1 layer silicates. *Clays and Clay Minerals*, **43**, 718–731.

Drits, V.A., Sakharov, B.A., Lindgreen, H., and Salyn, A.L. (1997a) Sequential structure transformation of illite-smectite-vermiculite during diagenesis of Upper Jurassic shales

from the North Sea and Denmark. *Clay Minerals*, **32**, 351–371.

Drits, V.A., Środoń, J., and Eberl, D.D. (1997b) XRD measurements of mean crystallite thickness of illite and illite/smectite: Reappraisal of the Kübler index and the Scherrer equation. *Clays and Clay Minerals*, **45**, 461–475.

Drits, V.A., Lindgreen, H., Salyn, A.L., Ylagan, R., and McCarty, D.K. (1998) Semiquantitative determination of trans-vacant and cis-vacant 2:1 layers in illites and illite-smectites by thermal analysis and X-ray diffraction: *American Mineralogist*, **83**, 1188–1198.

Drits, V.A., Lindgreen, H., Sakharov, B.A., Jakobsen, H.J., Salyn, A.L. and Dainyak, L.G. (2002a) Tobelitization of smectite during oil generation in oil-source shales. Application to North Sea illite-tobelite-smectite-vermiculite. *Clays and Clay Minerals*, **50**, 82–98.

Drits, V.A., Sakharov, B.A., Dainyak, L.G., Salyn, A.L., and Lindgreen, H. (2002b) Structural and chemical heterogeneity of illite-smectites from Upper Jurassic mudstones of East Greenland related to volcanic and weathered parent rocks. *American Mineralogist*, **87**, 1590–1607.

Drits, V.A., Lindgreen, H., Sakharov, B.A., Jakobsen, H.J., and Zviagina, B.B. (2004) The detailed structure and origin of clay minerals at the Cretaceous/Tertiary boundary, Stevns Klint (Denmark). *Clay Minerals*, **39**, 367–390.

Dunoyer de Segonzac, G. (1970) The transformation of clay minerals during diagenesis and low-grade metamorphism: A review. *Sedimentology*, **15**, 281–346.

Ferrage, E., Tournassat, C., Rinnert, E., Charlet, L., and Lanson, B. (2005a) Experimental evidence for Ca-chloride ion pairs in the interlayer of montmorillonite. An XRD profile modeling approach. *Clays and Clay Minerals*, **53**, 348–360.

Ferrage, E., Lanson, B., Sakharov, B.A., and Drits, V.A. (2005b) Investigation of smectite hydration properties by modeling experimental X-ray diffraction patterns: Part I. Montmorillonite hydration properties. *American Mineralogist*, **90**, 1358–1374.

Foscolos, A.E. and Powell, T.G. (1979) Mineralogical and geochemical transformation of clays during burial diagenesis (catagenesis): relation to oil generation. Pp. 261–270 in: *Proceedings of the International Clay Conference, Oxford* (M.M. Mortland and V.C. Farmer, editors). Developments in Sedimentology, **27**. Elsevier, Amsterdam.

Hanan, M.A., Totten, M.W., Hanan, B.B., and Kratochovil, T. (1998) Improved regional ties to global geochronology using Pb-isotope signatures of volcanic glass shards from deep water Gulf of Mexico ash beds. *Gulf Coast Association of Geological Societies Transactions*, Volume XLVIII, 95–106.

Hoffman, J.C. (1979) An evaluation of potassium uptake by Mississippi-river-borne clays following deposition in the Gulf of Mexico. PhD thesis, Case Western Reserve University, 169 pp.

Howard, S.A. and Preston, K.D. (1989) Profile fitting of powder diffraction patterns. Pp. 217–276 in: *Modern Powder Diffraction* (D.L. Bish and J.E. Post, editors). Reviews in Mineralogy, **20**, Mineralogical Society of America, Washington, D.C.

Hower, J., Eslinger, E., Hower, M., and Perry, E. (1976) Mechanism of burial metamorphism of argillaceous sediments: I. Mineralogical and chemical evidence. *Geological Society of America Bulletin*, **87**, 725–737.

Huang, W.-L, Longo, J.D., and Pevear, D.R. (1993) An experimentally derived kinetic model for smectite-to-illite conversion and its use as a geothermometer. *Clays and Clay Minerals*, **41**, 162–77

Huggett, J.M. and Cuadros, J. (2005) Low-temperature illitization of smectite in the late Eocene and early Oligocene of the Isle of Wight (Hampshire basin), U.K. *American Mineralogist*, **90**, 1192–1202.

Hunt, J.M. (1979) *Petroleum Geochemistry and Geology.* W.H. Freeman & Co., San Francisco.

Inoue, A., Velde, B., Meunier, A., and Touchard, G. (1988) Mechanism of illite formation during smectite-to-illite conversion in a hydrothermal system. *American Mineralogist*, **73**, 1325–1334.

Jackson, M.L. (1985) *Soil Chemical Analysis – Advanced Course*, 2nd edition, 11th printing. Published by the author, Madison, Wisconsin 53705, USA.

Kerr, D.R. and Grigsby, J.G. (1991) Recognition and implications of volcanic glass detritus in the fluvial deposits of the middle Frio Formation, South Texas. *Transactions, Gulf Coast Association of Geological Societies*, **XLI**, 353–358.

Lanson, B., Sakharov, B.A., Claret, F., and Drits, V.A. (2005) Diagenetic evolution of clay minerals in Gulf Coast shales: New insights from X-ray diffraction profile modelling. *13th International Clay Conference*, Tokyo, Japan, p. 39.

Lindgreen, H., Drits, V.A., Sakharov, B.A., Salyn, A.L., Wrang, P., and Dainyak, L.G. (2000) Illite-smectite structural changes during metamorphism in black Cambrian Alum shales from the Baltic area. *American Mineralogist*, **85**, 1223–1238.

Lingreen, H., Drits, V.A., Sakharov, B.A., Jakobsen, H., Salyn, A.L., Dainyak, L.G., and Kroyer, H. (2002) The structure and diagenetic transformation of illite-smectite and chlorite-smectite from North Sea Cretaceous-Tertiary chalk. *Clay Minerals*, **37**, 429–450.

Lynch, L.F. (1996) Mineral/water interaction, fluid flow, and Frio sandstone diagenesis: Evidence from the rocks. *American Association of Petroleum Geologists Bulletin*, **80**, 486–504.

Lynch, L.F. (1997) Mineral/Water interaction, fluid flow, and Frio sandstone diagenesis: evidence from the rocks: reply. *American Association of Petroleum Geologists Bulletin*, **81**, 1536–1537.

McCarty, D.K. (2005) XRD pattern simulation of clays and geological interpretation. *Programs and abstracts, The Clay Minerals Society 42nd Annual Meeting*, Burlington, Vermont, USA.

McCarty, D.K., Drits, V.A., Sakharov, B.A., Zviagina, B.B., Ruffell, A., and Wach, G. (2004) Heterogeneous mixed-layer clays from the Cretaceous greensand, Isle of Wight, southern England. *Clays and Clay Minerals*, **52**, 552–575.

Moore, D.M. and Reynolds, R.C. Jr. (1997) *X-ray Diffraction and the Identification and Analysis of Clay Minerals*, 2nd edition. Oxford University Press, New York.

Omotoso, O., McCarty, D.K., Hiller, S. and Kleeberg, R. (2006) Some successful approaches to quantitative mineral analysis as revealed by the 3rd Reynolds Cup contest. *Clays and Clay Minerals*, **54**, 751–763.

Perry, E. and Hower, J. (1970) Burial diagenesis in Gulf Coast pelitic sediments. *Clay and Clay Minerals*, **18**, 165–177.

Pevear, D.R., Williams, V.E., and Mustoe, G.E. (1980) Kaolinite, smectite, and K-rectorite in bentonites: Relation to coal rank at Tulameen, British Columbia. *Clays and Clay Minerals*, **28**, 241–254.

Pollastro, R.M. (1993) Consideration and applications of the illite/smectite geothermometer in hydrocarbon-bearing rocks of Miocene to Mississippian age. *Clays and Clay Minerals*, **41**, 119–133.

Righi, D., Velde, B., and Meunier, A. (1995) Clay stability in clay-saturated soil systems. *Clay Minerals*, **30**, 45–54.

Sakharov, B.A., Lindgreen, H., Salyn, A.L., and Drits, V.A., (1999) Determination of illite-smectite structures using multispecimen X-ray diffraction profile fitting. *Clays and Clay Minerals*, **47**, 555–566.

Shutov, V.D., Drits, V.A., and Sakharov, B. (1969) On the

mechanism of a post sedimentary transformation of montmorillonite into hydromica. *Proceedings of the International Clay Conference*, Tokyo. Israel University Press, pp. 523–531

Środoń, J. (1980) Precise identification of illite/smectite interstratifications by X-ray powder diffraction. *Clays and Clay Minerals*, **28**, 401–411.

Środoń, J. (1981) X-ray identification of randomly interstratified illite-smectite in mixtures with discrete illite. *Clay Minerals*, **16**, 297–304.

Środoń, J. (1984) X-ray powder diffraction identification of illitic materials. *Clays and Clay Minerals*, **32**, 337–349.

Środoń, J. (1999a) Use of clay minerals in reconstructing geological processes: recent advances and some perspectives. *Clay Minerals*, **34**, 27–37.

Środoń, J. (1999b) Nature of mixed-layer clays and mechanisms of their formation and alteration. *Annual Review of Earth and Planetary Science*, **27**, 19–53.

Środoń, J., Eberl, D.D., and Drits, V.A. (2000) Evolution of fundamental-particle size during illitization of smectite and implications for reaction mechanism. *Clays and Clay Minerals*, **48**, 446–456.

Środoń, J., Drits, V.A., McCarty, D.K., Hsieh, J.C.C., and Eberl, D.D. (2001) Quantitative X-ray diffraction analysis of clay-bearing rocks from random preparations. *Clays and Clay Minerals*, **49**, 514–528.

Środoń, J., Clauer, N., and Eberl, D.D. (2002) Interpretation of K-Ar dates of illitic clays from sedimentary rocks aided by modeling. *American Mineralogist*, **87**, 1528–1535.

Velde, B. and Peck, T. (2002) Clay mineral changes in the Morrow experimental plots, University of Illinois. *Clays and Clay Minerals*, **50**, 364–370.

Ylagan, R.F., Altaner, S.P., and Pozzuoli, A. (2000) Reaction mechanisms of smectite illitization associated with hydrothermal alteration from Ponza island, Italy. *Clays and Clay Minerals*, **48**, 610–631.

(*Received 22 June 2007; revised 11 March 2008; Ms. 0043; A.E. B. Lanson*)